Lab on a Chip

PAPER

View Article Online
View Journal | View Issue

Check for updates

Cite this: *Lab Chip*, 2026, **26**, 3229

Cell therapy manufacturing at full clinical scale: enhancing the quality CAR-T cell therapy starting materials through massively parallel automated microfluidic cell sorting

Alison M. Skelley, *[ab] Yasna Behmardi,[a] Luke F. Peterson,[a] David W. Inglis, [c] Mabel Shehada,[a] Laurissa Ouaguia,[a] Khushroo Gandhi,[a] Roberto Campos-González[a] and Tony Ward[a]

Autologous CAR-T cell therapy has demonstrated remarkable clinical efficacy in hematologic malignancies, yet its broader application remains limited by complex, labor-intensive cell therapy manufacturing and inconsistent product quality. We describe a novel microfluidic cell separation platform based on deterministic lateral displacement (DLD), integrated into a fully automated, closed-system instrument (Curate system). N = 150 leukopacks were processed at a flow rate of 400 mL h^{-1} with processed volumes up to 250 mL, white blood cell concentrations up to 168 M mL^{-1} and total white blood cell counts up to 24 billion white blood cells. Compared to Ficoll®-based density gradient centrifugation, microfluidic DLD processing yielded significantly higher leukocyte recovery (88% *vs.* 58%), superior platelet and red blood cell depletion, and reduced $CD69^+$ T cell activation. Flow cytometric analysis revealed improved phenotypic preservation across key T cell subsets, including naïve and central memory populations. Cytokine profiling demonstrated enhanced washing efficiency, with markedly lower levels of biologic response modifiers. DLD-purified T cells exhibited enhanced expansion kinetics and greater yield, supporting improved manufacturing outcomes. These findings position microfluidic DLD-based processing as a clinically relevant, scalable alternative to conventional methods, with potential to improve consistency, potency, and accessibility of CAR-T therapies.

Received 23rd January 2026,
Accepted 29th March 2026

DOI: 10.1039/d6lc00072j

rsc.li/loc

Open Access Article. Published on 02 April 2026. Downloaded on 6/16/2026 12:17:03 AM.
This article is licensed under a Creative Commons Attribution-NonCommercial 3.0 Unported Licence.

Introduction

Autologous cell therapy has seen accelerated progress towards eliminating blood cancers using patient derived engineered T cells. Unfortunately, the reality is that current therapies remain far from accessible for most patients, with costs that can reach upwards of $500 000.[1–3] Despite therapies being available since 2017, and with 9 therapies currently on the market, fewer than 40 000 patients have been treated.[4] One major hurdle is the very manual and lengthy cell therapy manufacturing process. Typical manufacturing protocols first perform a debulking step to purify white blood cells (WBCs) from an apheresis product, followed by T cell isolation using immunomagnetic beads. The T cells are then genetically engineered followed by expansion in culture to achieve the desired number of cells. Patient leukapheresis collections frequently contain the minimum number of T cells to create multiple therapeutic doses, but due to the inefficiencies of the manufacturing process, multiple days of *ex vivo* expansion are required to achieve the desired number of cells.[5] Several steps in the process require manual manipulation of the sample, and cell therapy manufacturing facilities commonly do not have the capacity or staff to manufacture more than a few therapies at a time.[6] As a result, strict evaluation criteria for patient eligibility and long wait times – upwards of 6 months – are a common reality.[6] Biological variability in starting materials and complex manufacturing processes result in inconsistent therapeutic outcomes; furthermore, up to 4–7% of manufacturing processes fail and patients never receive their therapy.[7] From a clinical perspective, cell therapy is often a therapy of last resort, and yet a significant portion of patients may require additional apheresis collections, bridging therapy, or because of a failed manufacturing process may not get their therapy at all.[8,9]

In typical CAR-T cell manufacturing, an initial debulking step is performed post-apheresis collection and prior to T cell selection and activation. Commonly used systems include

[a] *Curate Biosciences, USA*
[b] *Zeon Specialty Materials, 25 Metro Drive, Suite 238, San Jose, CA 95110, USA. E-mail: alison.skelley@zeonsmi.com*
[c] *School of Engineering, Macquarie University, Sydney, NSW 2109, Australia*

Open Access Article. Published on 02 April 2026. Downloaded on 6/16/2026 12:17:03 AM. This article is licensed under a Creative Commons Attribution-NonCommercial 3.0 Unported Licence.

density gradient centrifugation (Sepax™ C-Pro, Cytiva), counterflow centrifugation (Gibco™ CTS™ Rotea™, Thermo Fisher Scientific), and spinning membrane instruments (Lovo®, Fresenius Kabi). Although these instruments recover WBCs, they do so with variable cell losses, and with variable removal of erythrocytes and/or platelets. Contamination with platelets can alter the T cells and suppress proliferation during culture.[10] It is also widely known that centrifugation induces stress and non-desirable cell to cell interactions.[11–13] Additional treatment with ammonium chloride to lyse remaining erythrocytes can also negatively impact cell quality.[13–15]

Recent studies are linking cell quality with therapeutic outcomes. Lower levels of functional exhaustion markers in apheresis starting materials corresponded with a higher likelihood of therapeutic success.[16] Longer *ex vivo* culture time was associated with differentiated T cells and depletion of stem cell memory (T_{scm}) and naïve phenotypes,[17] potentially leading to poor efficacy due to T cell exhaustion and apoptosis.[18] Higher percentages of central memory T cells (T_{CM})[19,20] and lower levels of regulator T cells (T_{REG})[21] resulted in greater *in vivo* persistence and greater anti-tumor activity. While alleviation of manufacturing hurdles and cost reduction is a primary focus, careful attention must be given to optimizing cell quality both into and out of the manufacturing process to achieve the best therapeutic outcome.

Novel microfluidic technologies are showing promise for improving the cell therapy manufacturing process. High-throughput purification of WBCs from blood and blood products has been demonstrated by numerous different technologies including deterministic lateral displacement (DLD),[22] spiral inertial microfluidics,[23] multi-channel inertial designs,[24] inertial separation arrays[25,26] and other passive, active, and hybrid approaches.[27] Other technologies are focused on later stages of the manufacturing process, including T cell isolation, transfection and expansion.[28,29] While these technologies have demonstrated greater efficacy than their non-microfluidic counterparts, and may be optimized for high throughput operation, very few, if any of the technologies have demonstrated full clinical-scale operation from leukopacks (apheresis collections), operating at hundreds of mL and manipulating billions of cells.

Previously, we described a microfluidic chip that used the principles of deterministic lateral displacement (DLD) to process blood and blood products for the production of CAR-T cells.[30,31] This manually operated proof-of concept scale device demonstrated superior purification and phenotypic advantages in the microfluidic product compared to density gradient centrifugation. In this paper, we focus on the next generation of microfluidic DLD cell separation devices, optimized and scaled up to process full leukopacks (standard apheresis units with volumes of up to 250 mL) within an hour. We also describe the integration of these massively parallel microfluidic arrays into a novel single-use disposable cassette and its use on an easy-to-use automated prototype system. We characterize the performance of this system through head-to-head runs with density gradient centrifugation (one of the most widely used methods for debulking post-apheresis) and show the functional benefits of cells isolated using the microfluidic approach.

Materials and methods

Microfluidic DLD device and cassette fabrication

DLD microarrays were constructed with a ZEONEX® Cyclo Olefin Polymer (COP, Zeon Corporation) *via* compression molding (Edge Precision Manufacturing, a Zeon Corporation subsidiary). Molded arrays were lidded with a COP film by solvent bonding. Manifold layers were prepared by heat staking hydrophobic vents at the terminus of each manifold channel. These vents facilitated air leaving during the priming operation. Paired lidded elements were laser welded on each side of the central manifold layer. Single barbed tubing connections were made for each of the 4 manifold channels (sample, running buffer, product and waste). Two manifold units (net 4× microfluidic layers) were connected together *via* barbed y-connectors and then connected to the cassette *via* a single set of inputs and outputs. The cassettes were created by laser welding a thin film to the front side and back side of an injection molded cassette body (FastRadius). Compression-molded gaskets were placed into the cassette and held in place using a laser-welded gasket frame. Tubing to connect to the various reagent and sample/product/waste bags was secured to the cassette *via* UV glue. Tubes were terminated either in a bag spike or with a sealed end. The sample tube featured an in-line capsule filter with a 20 μm nylon membrane (Clear Solutions). Peristaltic tubing was connected to the barbed pump tube connectors on board the cassette. The fully closed cassette was sterilized using ethylene oxide prior to use.

Curate system

The Curate system featured 4 independent peristaltic pumps for sample, diluent (allowing in-line dilution), buffer, and waste. Independent control enabled precise management of flow rates, relative ratios and fluid viscosities to establish optimized DLD operations for apheresis processing. Fluid routing was controlled by a series of solenoid valves aligned with gaskets on the cassette. Bags for the sample, product, and waste were hung on load cell equipped hangers, which verified fluid movements in and out of the DLD array. Pressure and bubble sensors on the instrument were used to monitor the separation process and trigger adjustments to maintain fluid ratios or prevent air ingress as needed.

Running buffers

DLD microarrays were primed using 0.6% F-127 in saline. A priming concentrate of 10% F-127 in water was sterile filtered and then bottled; these bottles were then autoclaved prior to storage at 4 °C. Before the run, 15 mL of the concentrate was withdrawn from the bottle and injected into a 250 mL bag of

 This journal is © The Royal Society of Chemistry 2026

Open Access Article. Published on 02 April 2026. Downloaded on 6/16/2026 12:17:03 AM. This article is licensed under a Creative Commons Attribution-NonCommercial 3.0 Unported Licence.

sterile saline (VWR, cat. no. 95037-334) which was then connected to the cassette.

Running buffers were consisted of an albumin mixture in phosphate-buffered saline (PBS) or Plasma-Lyte®-A Injection, pH 7.4 (PLA, VWR cat. no. 80089-818). Concentrated bovine serum albumin (BSA) or human serum albumin (HSA, Grifols Albumin (Human) 25%, USP, Plasbumin®-25, cat. no. 13533-692-71) was injected into bags of sterile PLA or added to PBS and sterile filtered. The optimal final protein concentration was 2–4%. In some runs, cell culture media were used, such as TexMACS™ (Miltenyi Biotec) or CTS™ OpTmizer™ (Thermo Fisher Scientific). If reagents were prepared more than a day prior to run, they were sterile filtered (0.2 μm pore size) and then loaded into sterile bags. Sterile collection bags for the product and waste were connected to the cassette prior to use *via* tube welding.

Cell counting

All samples, inputs, products, waste and cells in culture were counted with a Cell-Dyn Emerald 22 (Abbott). The hematology analyzer provides absolute numbers of the different blood cell types plus other hematologic parameters.

Sample pre-treatment

Leukopack (LKP) samples (standard apheresis units) were obtained from apheresis of normal donors (San Diego Blood Bank, Red Cross Los Angeles, Stem Express (now CGT Global), or HemaCare). Upon collection, leukopacks were spiked with an additional amount of Anticoagulant Citrate Dextrose Solution, Solution A (ACD-A) for a final citrate concentration of 19 mM then transported at 4–8 °C. LKPs were stored overnight at 2–8 °C on an Ohaus rocker with constant movement. Before use, the LKPs were brought back to room temperature.

A benzonase pre-treatment was performed prior to processing the samples. Benzonase nuclease HC (final concentration 50 units mL^{-1}, Millipore, cat. no. 71205-3) and $MgCl_2$ (final concentration 5 mM) were added to the leukopack followed by 1 h incubation at room temperature while rocking. Before processing, EDTA (final concentration 5 mM) was added followed by another 15 min incubation at room temperature.

All samples used in this study were purchased from commercial organizations that collect healthy donor blood and apheresis materials under the IRB-approved protocols in compliance with the U.S. Department of Health & Human Services regulations (45 CFR 46). The IRB protocols included documented informed consent and privacy and confidentiality protections in compliance with HIPAA and 21 CFR Part 50. All donors provided informed consent to the various commercial organizations for the collection and use of their blood for research purposes, and all samples were de-identified prior to purchase. This study is considered exempt from IRB oversight and approval because the use of de-identified samples does not constitute human-subjects research.

https://grants.nih.gov/grants/policy/hs/private-information-biospecimens-flowchart.pdf.

Manual density gradient separation

Purification of PBMC with Ficoll-Paque® (Cytiva cat. no. 17544202) was performed using the manufacturer's instructions.[32] Briefly, 10–20 mL of the leukopack was diluted 1 : 1 in cell culture media and layered on top of an equal volume of Ficoll®. The sample was centrifuged at 400× *g* for 35 min with no break. The PBMC layer was carefully removed using a pipet. The PBMC layer was washed *via* resuspending in 50-fold excess media, followed by pelleting by centrifugation at 400× *g* for 10 min (wash 1). The pellet was again resuspended in 50-fold excess media and then centrifuged at 200× *g* for 10 min (wash 2). The final pellet (PBMC) was resuspended in media to the original volume. This manual process took ~1.5 h to process only 10–20 mL of the initial sample.

T cell stimulation and expansion

Purified cells either from Ficoll® or microfluidic cell sorting were counted and the T cell number was determined before activation and culture. Cells were normalized to a concentration of 10×10^6 mL^{-1} in TexMACs™ media and then were incubated with pre-washed CD3/CD28 magnetic beads (Dynabeads™, Thermo Fisher Scientific, cat. no. 11161D) at a ratio of 3 : 1 beads per T cell for 1 h at 37 °C.[33] After the incubation, the bead/cell slurry was placed in a magnet for 5 minutes and then the supernatant was discarded. The slurry was resuspended to a T cell concentration of

1×10^6 mL^{-1}, or the desired concentration, in full media containing TexMACs™, 10% fetal bovine serum (FBS, Phoenix Scientific, PS-100) or 5% HSA, plus 5 ng mL^{-1} of IL-7 and IL-15 (Biolegend cat no. 777704 and 570308), and 1% penicillin/streptomycin (Thermo Fisher Scientific cat. no. 15140122). The cells were plated in 6-well GRex plates or 1 L G-Rex containers (Wilson Wolf Manufacturing cat. no. 80240 M and RU81100 respectively) and placed at 37 °C and 5% CO_2 in a humidified incubator.

FACS cell analysis

Phenotypic analysis and growth of cultured T cells were measured post-purification and at different days post-transduction. Cells in culture were sampled by mixing the cells, taking an aliquot and then detaching magnetic beads by repeated pipetting and placing the mixture in a magnet for 5 min.[33] Cells were counted with a CellDyn hematology analyzer (Abbott). Staining for flow cytometry was done using 0.5–1.0 × 10^6 cells resuspended in 100 μL of 0.5% BSA/PBS. Cells were stained in the dark for 30 min with the corresponding panel(s) of antibodies, followed by a wash (for the 9-color panels) and then fixed with 1.0% *p*-formaldehyde (if necessary) before reading in a Novocyte flow cytometer (Agilent Technologies). Data analysis was done with NovoExpress software (Agilent

Open Access Article. Published on 02 April 2026. Downloaded on 6/16/2026 12:17:03 AM.
This article is licensed under a Creative Commons Attribution-NonCommercial 3.0 Unported Licence.

Technologies). Concentration optimized panels used for phenotypic analysis are detailed in the SI.

Cytokine analysis

Cytokines present in the source material and in products of each separation method were quantified. Ficoll® products (standard 2-wash protocol) and DLD products were collected following processing. Aliquots were removed and normalized to 10^7 total WBC cells. The aliquots were centrifuged and then the supernatant was removed for analysis. DLD products were prepared with microfluidic devices operated by a pressure-driven controller (Fluigent). Supernatants were frozen into cryo-vials at −80 °C as soon as practical following each separation and supernatant isolation process. Controls of the different matrices/buffers were also sampled and frozen at the same time. Cryopreserved samples were sent to Eve Technologies for a 51-plex Discovery Panel Luminex analysis targeted to a broad range of cytokines, chemokines and cell damage related biomarkers known to be associated with the inflammation cascade (analytes are shown in Table S1).

Results

Microarray design

The microfluidic cell sorting system utilizes deterministic lateral displacement (DLD, also called deterministic cell sorting or DCS) to separate cells by size. The DLD principle relies on precisely constructed micropost arrays that are tilted with respect to the major flow direction. The microarray has a critical diameter (D_C) determined by the basic array parameters of array tilt and gap sizes.[34] As shown in Fig. 1A, cells with diameters greater than the critical diameter are deflected and travel along the direction of the array while cells with diameters less than the D_C are unimpeded by the array and flow straight through. In order to both separate and wash the cells into a clean collection buffer, each array contains co-flowing input streams of both the sample and buffer (also referred to as wash buffer). The location of the boundary is dictated by the ratio of input streams. With only laminar flow in the array, there is no turbulent mixing at the boundaries, and diffusion is limited by the ~1 second residence time. For the device utilized here, a D_C of ~4 μm was selected to deflect all white blood cells to the product, while platelets and red blood cells traveled straight through to waste. Red blood cells (RBCs) traveled through the array on their short axis and thus behaved like ~2 μm objects, passing through the array to the waste collection bag.

The array used a mirrored geometry to maximize the concentration of the collected product, with two arrays on either side of a central collection channel (also called a bypass channel, Fig. 1B). As cells were deflected by the arrays, they moved towards the central collection channel. Only cells

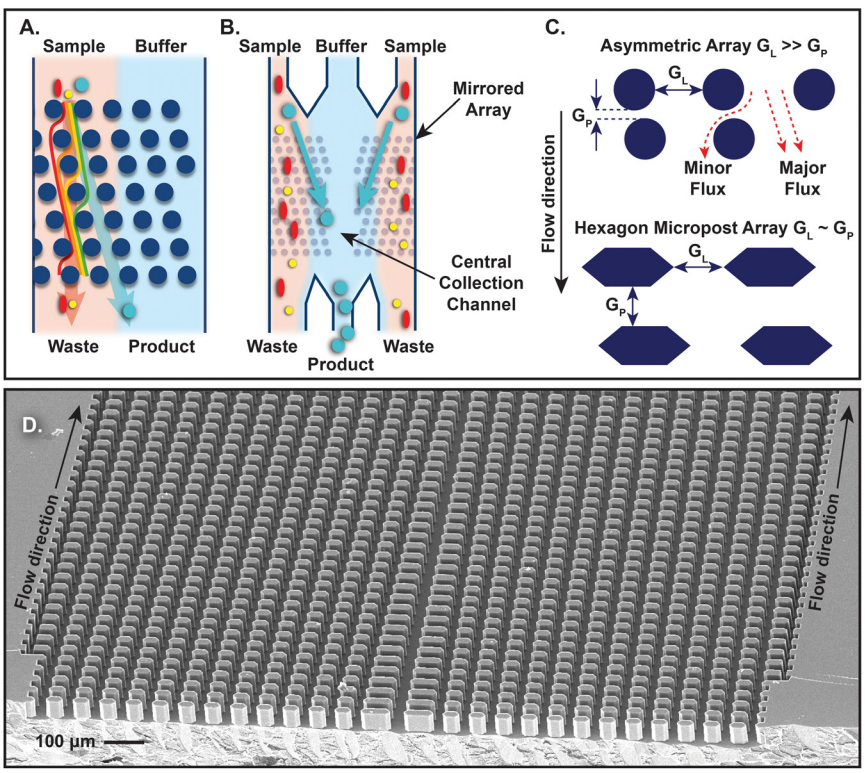

Fig. 1 A) Principle of DLD separation. When cells flow through an array that is tilted with respect to the major flow direction, they are fractionated by size. Large objects are deflected and follow the array direction while small objects travel straight through. B) Operation of a mirrored array, with larger product cells collected in a central collection channel. C). Asymmetric hexagon array geometry that maintains higher throughput while eliminating small gaps. D) SEM image of the hexagonal array fabricated in plastic using compression molding. Arrows indicate the direction of the flow.

 This journal is © The Royal Society of Chemistry 2026

Open Access Article. Published on 02 April 2026. Downloaded on 6/16/2026 12:17:03 AM.
This article is licensed under a Creative Commons Attribution-NonCommercial 3.0 Unported Licence.

and fluid in this central collection channel and immediately adjacent columns were collected as products, and the remainder of the fluid in the array went to waste. A small portion of the buffer was also rejected to waste to make sure that the collected product was free of diffusible species that may have crossed the boundary.

The design of the micropost array was optimized for throughput and capacity, anticipating the high concentrations of cells present in apheresis samples. To improve throughput per lane, we created an asymmetric DLD array[35] with wider gaps perpendicular to the flow direction (also referred to as the lateral gap, or G_L) and narrower gaps parallel to the flow direction (also called the downstream gap, or G_D). Widening the lateral gaps between microposts reduced the fluidic resistance within the array and had the benefit of making the array more resistant to biofouling. We also reduced the spatially average shear rate on the cells by using microposts with sharp vertices facing into the gap[22,36] (SI). To maintain the D_C of ~4 μm while avoiding unnecessarily small gaps, a challenge for high-volume manufacturing of microfluidic devices, we used microposts with a hexagonal cross-section (as-fabricated: 18.8 × 39.2 um). This created an asymmetric gap profile (thus minimizing the flow lane width in the minor flux direction) but did so by elongation as opposed to constriction (Fig. 1C). The downstream gap between faces of the hexagon posts (G_D) was 16.2 μm, and the lateral gap between the corners of the hexagons (G_L) was 21.8 um. These feature sizes were well within the manufacturability limits for compression molding as shown by the SEM photo of the mirrored array constructed with COP plastic (Fig. 1D).

The optimal array tilt angle was a tradeoff between gap size, array length and multi-lane manufacturability. Arrays with a smaller tilt angle (lower horizontal shift of microposts between rows and the net larger number of rows per repeating array unit) result in narrower flow lanes following the minor flux direction. This directly correlates with a smaller functional D_C. However, smaller array tilt angles also require longer DLD arrays to obtain the same lateral displacement of cells. We wanted to fabricate numerous lanes on a 6″ wafer which limited the maximum array length, especially near the perimeter of the wafer. We also wanted to increase the redundancy of the array, creating an array with ~2× the required length to transit from the negative to positive boundary. While this modification did increase fluidic resistance, there was a positive impact on net recovery when processing higher cell concentrations from apheresis materials, allowing extra time to collect cells that had been bumped off their trajectory due to cell–cell interactions in the array. A tilt slope ε of 1/34 radians was chosen as a compromise of maintaining larger gaps and enabling a 2× redundancy while also keeping the net array length under 42 mm.

We calculated the D_C using Zeming *et al.*'s[35] method for calculating an effective epsilon ($\varepsilon_{effective}$) that factors in different gaps downstream (parallel) *vs.* lateral (perpendicular) to flow directions. The equation uses a ratio of the downstream (P_D) *vs.* lateral pitch (P_L), where the pitch is the sum of the gap plus post size (width or length) in that direction:

$$\varepsilon_{\text{effective}} = \frac{(P_{\text{Downstream}})\tan(\theta)}{(P_{\text{Lateral}})}$$

$$P_{\text{Lateral}} = \text{Gap}_L + \text{Post}_L$$

where P_D = 35 um, P_L = 61 um, and $\tan(\theta)$ = 1/34.

We then used the D_C equation from Inglis *et al.*:[34]

$$D_C = 1.4 \times G_L \times \varepsilon^{0.48}$$

which resulted in an as-fabricated critical diameter of 4.3 μm.

An additional feature was added at the inlet of each lane to help minimize the impact of any biofouling. A partial separator wall[37] was added between the sample and buffer arrays, extending only 7.8 mm down from the array inlet (Fig. 2A). This distance was short enough relative to the full length (41.5 mm) to have no impact on cells transiting into the central collection channel. The separator wall compartmentalized any biofouling at the entrance to the array and prevented the sample from spilling over into the buffer stream and contaminating the product. At the terminus of the separator wall, guide posts were used to keep fluid streams organized as the arrays were merged into one larger array.

Both positive boundaries (the central collection channel and outer edge of the separator wall) and negative boundaries (the outer edge of the bulk array; the inner wall of the separator channel) were adjusted to maintain array functionality. These boundary modifications were performed according to the methods of Inglis *et al.*, but with modifications to comply with minimum manufacturable gaps.[38,39] Standard boundary correction at the negative edge requires gaps that are considerably smaller than the main array gaps. These could not be manufactured, so the shape of some boundary obstacles was changed (squared and elongated) to yield a longer and higher resistance flow path for the minor flux. At the positive boundary, the posts were also elongated to both deliver the major flux into the central collection channel and then also slowly allow flow to escape back into the array in subsequent rows, creating a D_C that mimicked that of the bulk array (Fig. 2A, bottom). The boundaries were intentionally staggered such that row 1 for the negative boundary did not correspond with row 1 for the positive boundary. This prevented both major boundary adjustments from occurring in the same row.

Total system throughput and capacity were accomplished through massive parallelization, both in the number of lanes per layer and stacking multiple layers together. 34 lanes were fabricated in a single layer (Fig. 2B). Two of these layers were lidded and then laser welded to a central manifold layer containing a common set of manifold channels, one for each of the sample, buffer, product and

Open Access Article. Published on 02 April 2026. Downloaded on 6/16/2026 12:17:03 AM.
This article is licensed under a Creative Commons Attribution-NonCommercial 3.0 Unported Licence.

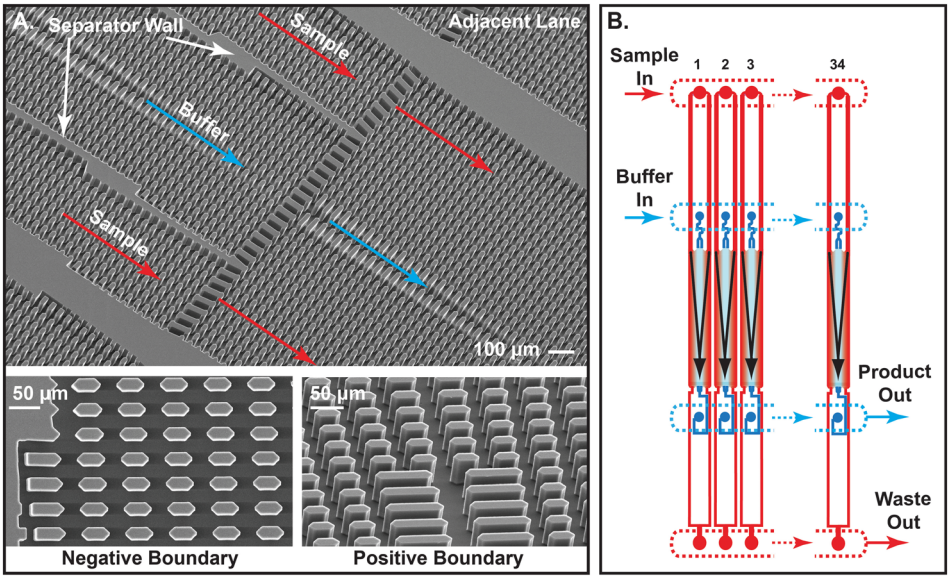

Fig. 2 A) Separator wall structure to compartmentalize any biofouling at the array inlet. Negative and positive boundary modifications to maintain the uniform critical diameter (and major/minor flux) at the channel walls and in the central collection channel. All SEM photos are of the compression molded, COP plastic device. B). Schematic of the parallelization strategy to increase total throughput. 34 lanes per layer share common manifold channels. Diagonal flow (inlet on one side, outlet on the other) enables identical flow paths regardless of lane, helping to ensure balanced flow across all lanes.

waste. Two of these manifold units were then connected in parallel with 4 y-connectors, one for each manifold channel. The result was 136 lanes across 4 microfluidic layers operating in parallel, with only 2 inputs and 2 outputs from the cassette. Even fluid distribution was accomplished by keeping the manifold channels large with low fluidic resistance relative to the array lanes. In addition, identical path lengths were maintained for each lane by feeding the sample and buffer into the manifold ahead of lane 1 and collecting the product and waste from the manifold after lane 34. The throughput of the final geometry was 1000 mL h^{-1}, with sample and buffer inputs comprising 400 mL h^{-1} and 600 mL h^{-1}, respectively, and product and waste outputs generated at 300 mL h^{-1} and 700 mL h^{-1}, respectively.

Curate system

Previously, a constant pressure-driven system was used to operate the proof-of-concept scale microfluidic device. However, maintaining sterility and preventing carryover contamination through the system was more easily guaranteed using a fully-closed cassette. The solution featured on the Curate system consisted of peristaltic pumps on the instrument and integrated peristaltic tubing on the sterile, fully-closed cassette, thus guaranteeing that the fluid never touched any instrument pump components (Fig. 3A and C). The system contained 4 independent pumps for the sample, diluent (allowing in-line dilution though not used in this study), buffer, and waste. Independent control enabled precise management of flow rates and relative ratios at both inlets and outlets to establish optimized DLD operations for apheresis processing.

Each pump rotor featured dual sets of rollers to minimize pulsatile flow, critical for establishing stable fluid boundaries between the sample and co-flowing buffer in the microfluidic array. Briefly, a single fluid line on the cassette was split into two paths, travelled through peristaltic tubing over two sets of rollers 180 degrees out of phase, and then was recombined, delivering smoother flow. The microfluidic array separator wall described above also helped suppress flow oscillations, maintaining a stable boundary once the fluid streams were combined into the wider array.

The Curate system featured 2 modes of operation (Fig. 3B). In the standard mode of operation (separation and wash), white blood cells were deflected into running buffer and collected in the product bag. The output volume of the product bag was very similar to the input volume of the sample (some adjustment due to priming and flushing steps). An alternative mode of operation increased the concentration of white blood cells in the product by recirculating the collected product back through the array as the collection buffer. This was facilitated by a recirculation path on the cassette (dashed lines, Fig. 3A) and easily controlled by actuating just 2 valves open/closed. This mode of operation, titled separation, wash and concentration, required no additional processing time and the output concentration was adjusted based on the downstream assay requirements. Load cells on all bag hangers allowed real-time monitoring of total fluid volumes and flow rates. Final target volumes for separation, wash and concentration were achieved by triggering the recirculation step based on the

 This journal is © The Royal Society of Chemistry 2026

Open Access Article. Published on 02 April 2026. Downloaded on 6/16/2026 12:17:03 AM.
This article is licensed under a Creative Commons Attribution-NonCommercial 3.0 Unported Licence.

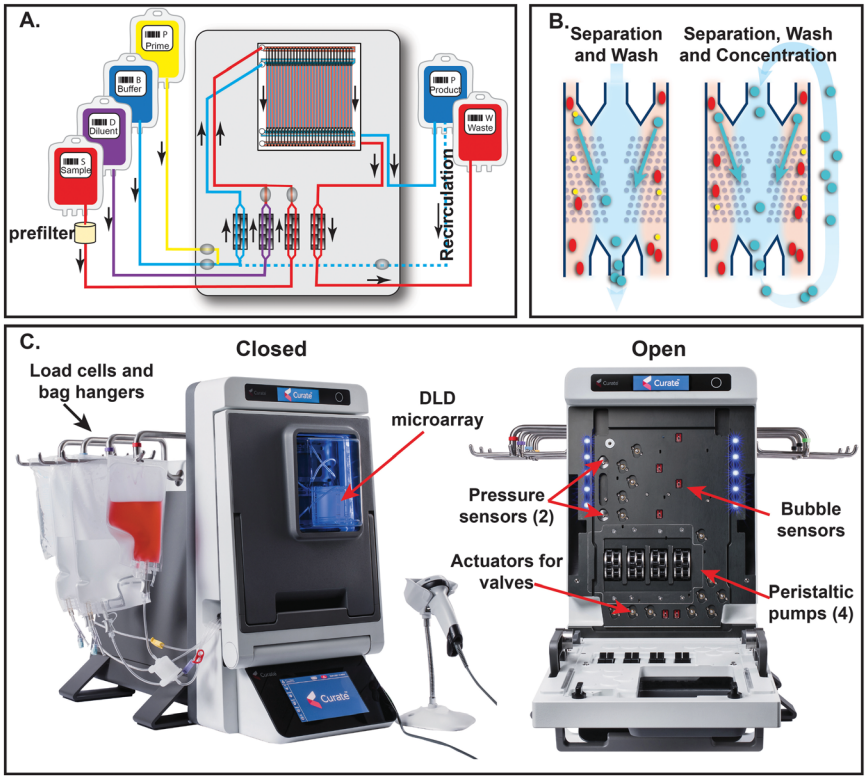

Fig. 3 The Curate system for automated microfluidic processing of apheresis samples. A) The fully closed cassette contained a microfluidic array as well as channels, valves and peristaltic tubing to direct fluid into and out of the separation unit. B) Different modes of operation. C) The Curate system operated the cassette *via* peristaltic pumps and solenoid valves while monitoring separation progress *via* load cells on the hangers and in-line pressure and bubble sensors.

load cell measurement for the product bag. Since the sample input volume was larger than the product output volume, there was a net decrease in product bag volume during recirculation. Thus, the optimal volume was achieved by actuating between run and recirculation modes, keeping the bag mass between an upper and a lower threshold. This flip/flop valve state continued until all the sample was processed, and enabled the same target output volume regardless of the input volume, without having any impact on processing time. An example of the sensor data for a recirculation run is shown in Fig. S3.

Performance of the microfluidic DLD cell separation system

The microfluidic cell sorting system processed undiluted apheresis samples at 400 mL h^{-1}, resulting in fully automated processing times of under an hour with minimal (~15 min) hands-on time up front. Apheresis collections from both Terumo Spectra Optia™ and Fresenius Kabi Amicus™ systems were processed, and example collected products and waste are shown in Fig. 4A. N = 150 normal donor apheresis collections (average volume of 150 ± 50 mL, maximum volume 245 mL) were processed undiluted to demonstrate the system's performance across a wide range of donor materials. The performance metrics are shown in Fig. 4B. The average % WBCs recovered was 88 ± 6%. The array process efficiency (cells in the product *vs.* all collected cells in product and waste bags) was much higher, with 97 ± 3% of all cells recovered in the product. The unrecovered cells (not in the product or waste) were likely trapped upstream of the microfluidic array by the in-line 20 μm pre-filter configured to remove cell clumps before they impacted array performance. The purity of the collected products was evaluated by measuring platelet (PLT) and red blood cell depletion (RBC). %PLT depletion was 99 ± 1% and %RBC depletion was 91 ± 7% respectively. Viability was determined by staining CD45+ cells with 7-AAD and was 96 ± 3%, equivalent to the input population. No difference in performance between separation and wash and separation, wash and concentration modes was observed (Fig. S2).

The key separation metrics of %WBC recovery and % process efficiency (product *vs.* waste) were evaluated for dependency on input concentration or on total cells processed. Surveying the N = 150 samples, leukopack concentrations up to 168 M mL^{-1} (average of 56 ± 24 × 10^6 M mL^{-1}), total WBC cellularity up to 24 billion leukocytes (average 8.5 ± 3.8 billion leukocytes) and volumes up to 245 mL (average of 150 ± 50 mL) were processed without dilution or modification of the protocol. While a slight decrease in %WBC recovery was observed with both increasing input concentrations and increasing input total WBCs processed, the % process efficiency showed no impact with very few

Open Access Article. Published on 02 April 2026. Downloaded on 6/16/2026 12:17:03 AM.
This article is licensed under a Creative Commons Attribution-NonCommercial 3.0 Unported Licence.

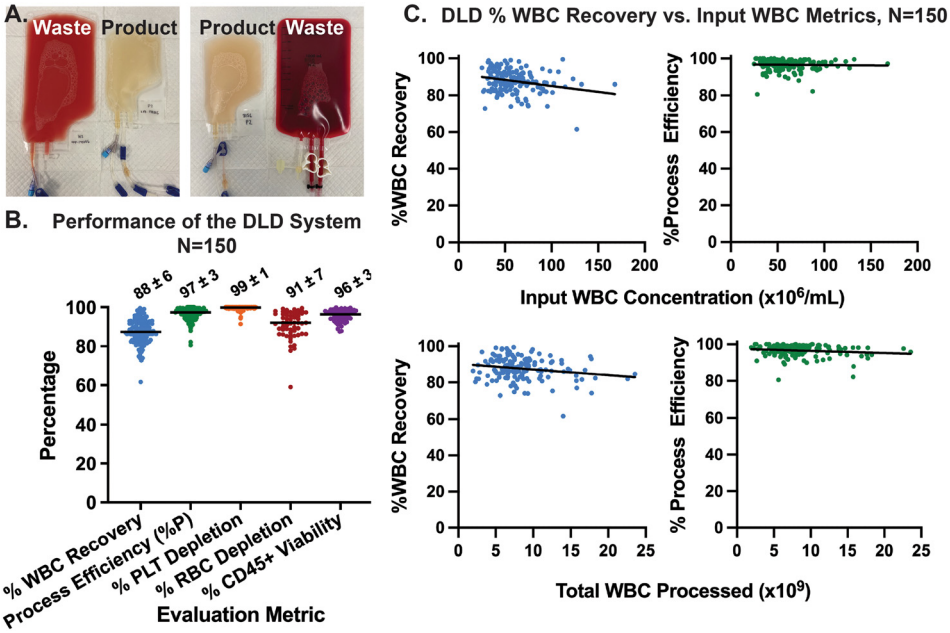

Fig. 4 A) Examples of microfluidic DLD products and waste generated by processing apheresis samples. B) The performance of the microfluidic DLD system across N = 150 samples evaluated by %WBC depletion, % process efficiency, %PLT depletion, %RBC depletion, and %CD45+ viability. Values indicate mean ± standard deviation and the horizontal line indicates the median value. C) %WBC recovery *vs.* input concentration (top) and *vs.* total WBCs processed (bottom). Calculated slopes are shown by the black lines. The %WBC recovery plots both had a slight downward trend, while the % process efficiency showed no significant trend.

WBCs in the waste fraction (*t*-test, deviation from 0 slope not significant). This indicates that with higher concentrations and/or total WBCs processed, there were more cells lost to the system, likely trapped in the upstream filter due to increased cell clumping that occurs at higher cell counts. Materials that passed the upstream filter were still separated with equivalent efficiency compared to lower concentrations and counts.

During the run phase, the in-line pressure detectors upstream of the DLD were used to monitor the run progress for any biofouling. If the pressure rose above 150 kPa then the system automatically scaled the total throughput from 1000 mL h^{-1} to 600 mL h^{-1}. If the pressure continued to rise and the next threshold of 170 kPa was passed, the system aborted the run and notified the user while flushing any sample in the cassette back into the sample bag. This remaining sample could then be loaded on a new cassette, if so desired by the operator. Of the 150 samples loaded, only 9 runs were auto scaled by the instrument, and of those runs, 7 ran to completion at the scaled flow rate of 240 mL h^{-1}. The other 2 runs still processed >85% of the sample before aborting and recovered >80% of the total white blood cells (WBCs) loaded. The performance metrics from those 9 runs are included in the N = 150 data set and details of a failed run, including sensor data, are described in the SI.

Recovery and depletion performance of microfluidic DLD *vs.* manual Ficoll-Paque®. The microfluidic DLD system processed full leukopacks within an hour. By comparison, processing the same volume by manual density-gradient centrifugation (Ficoll-Paque®) required up to 4 hours with significant hands-on time, increased contamination risks, and yielded operator dependent results. Performance of the system was tested against manual Ficoll® by processing the same set of leukopacks by each method, removing ~10% of the leukopack volume (10–20 mL) for Ficoll® and processing the remainder *via* the microfluidic system. Recoveries of each method for N = 86 split samples are shown in Fig. 5. Microfluidic DLD recovered 88 ± 7% of WBCs loaded while Ficoll® only recovered 58 ± 17%, indicating an average of ~1.5× more cells. The microfluidic system also showed an improvement in washing efficiency compared to manual density gradient centrifugation (Fig. 5, bottom left). The PLT depletion was ~10 fold better and significantly more consistent in DLD-processed samples, with a % depletion of 99 ± 1% for the microfluidic system *vs.* 91 ± 10% for Ficoll-Paque®. A subset of samples was stained and analyzed by flow cytometry to better quantify residual RBC and CD3+ T cell concentrations. Out of N = 45 samples, the RBC depletion was ~2-fold better in microfluidic DLD than Ficoll®. The recovery of CD3+ T cells showed similar trends to the %WBC recovery (Fig. 5, bottom right), with ~1.7× more CD3+ cells recovered by microfluidic DLD than by Ficoll®.

Relative purity of microfluidic DLD *vs.* manual Ficoll-Paque®. Microfluidic cell separation delivered higher WBC recovery coupled with greater RBC and PLT depletion, resulting in a purer WBC population of cells. The ratios of RBC/WBC and PLT/WBC are shown in Fig. 6A and B. Apheresis input ratios were calculated using the hematology analyzer measurements prior to processing. Product ratios were determined by staining for the different cell types and

 This journal is © The Royal Society of Chemistry 2026

Open Access Article. Published on 02 April 2026. Downloaded on 6/16/2026 12:17:03 AM.
This article is licensed under a Creative Commons Attribution-NonCommercial 3.0 Unported Licence.

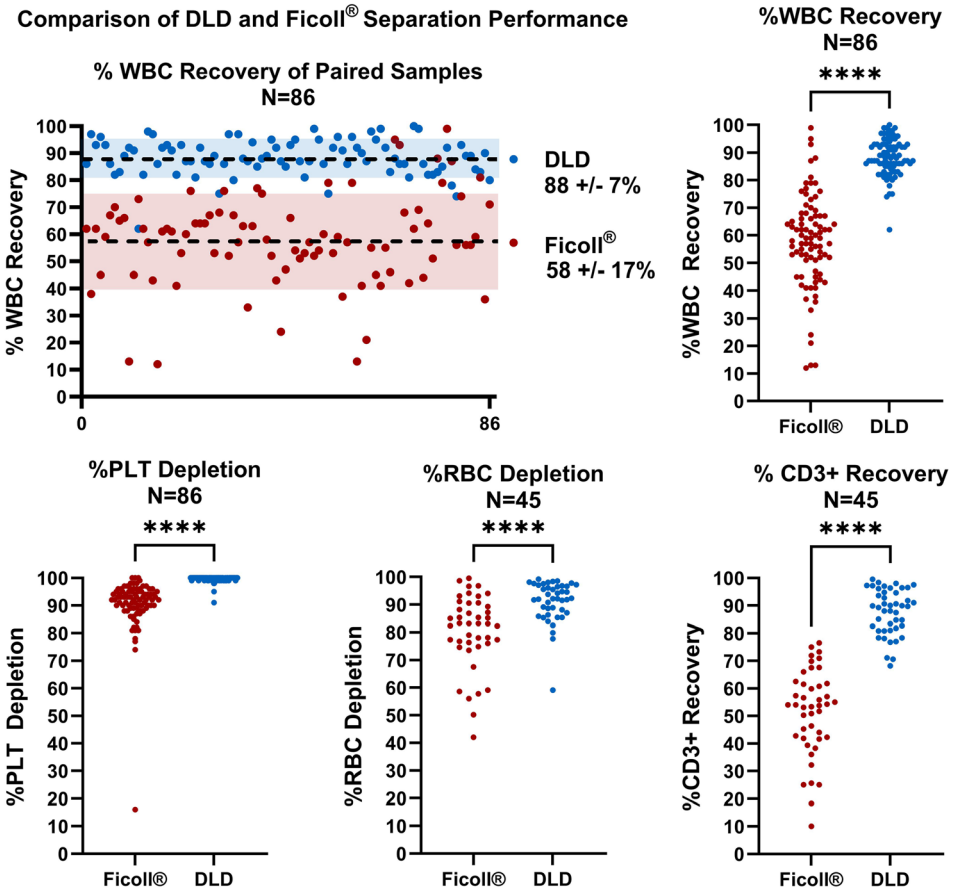

Fig. 5 Paired processing metrics of DLD *vs.* Ficoll® preparation methods.%WBC recovery, %PLT depletion, %RBC depletion and %CD3+ recovery were all significantly higher in the DLD system. RBC depletion and CD3+ recovery were determined by staining a random subset (N = 45) of the paired samples for FACS analysis. (****) = $p < 0.0001$, all comparisons are two-tailed t-tests. Horizontal lines indicate median values.

analyzing by flow cytometry. The microfluidic system reduced the RBC/WBC ratio by 70-fold, a greater than 2-fold improvement over Ficoll®. There was a more significant difference when comparing the PLT depletion, with microfluidic DLD achieving an average ~100-fold reduction in the PLT/WBC ratio, a ~10 fold improvement over Ficoll®. The combined impact was an improvement in purity from on average ~2% in the input material to only ~14% *via* Ficoll®, but over 60% by microfluidic processing.

T cell phenotype. Recent publications have shown that pre-activation negatively impacts the transformation to CAR-T cells, leading to loss of therapeutic potential.[17,18] Recognizing potential process differences with respect to cell : cell interaction and tonic signaling, N = 21 paired products were phenotyped by flow cytometry within two hours of processing. Of the N = 21 samples, N = 5 DLD samples were processed using pressure-driven flow to confirm that peristaltic pumping had no impact on activation in the microfluidic products. CD69+ was chosen as a marker to indicate activation levels in the cell population. Basal product activation state was measured prior to any cell engineering. As shown in Fig. 7A, the Ficoll® prepared cells had on average ~2× higher percentage of CD69+ T cells (p = 0.0018). The Ficoll® prepared cells also had more variability across the N = 21 samples, with one product showing >25% of the CD3+ cells that were also CD69+. No differences were observed between DLD products collected *via* peristaltic and pressure driven flows (SI).

A randomly-selected smaller subset of samples (paired, N = 8) were further phenotyped to investigate CD69+ expression within the T cell effector differentiation pathway subsets. The 4 major subtypes are naïve T cells (T_N, CCR7+CD95-CD45RA+), central memory T cells (T_{CM}, CCR7+CD95+CD45RA-CD62L+), effector memory T cells (T_{EM}, CCR7-CD95+CD45RA-CD62L-), and terminally-differentiated effector memory T cells (T_{EMRA}, CCR7-CD95+CD45RA+CD62L-).[40] Each of these subtypes play a different role when engineered with CAR-T, ranging from short-lived but potent effector function (T_{EM}) to long-lived *in vivo* expansion and proliferation (T_{CM}).[41] The %CD69+ was determined within each subtype and the plot is shown as a ratio of DLD-prepared cells *vs.* Ficoll®-prepared cells. Equivalent %CD69+ activation is indicated by the red dotted line (value = 1). In all subtypes analyzed, a similar pattern was observed. The Ficoll® prepared CD4+ and CD8+ cells on average showed higher %CD69+ activation, resulting in mean ratio values <1. Using a one-sample, two-tailed t-test with a

Open Access Article. Published on 02 April 2026. Downloaded on 6/16/2026 12:17:03 AM.
This article is licensed under a Creative Commons Attribution-NonCommercial 3.0 Unported Licence.

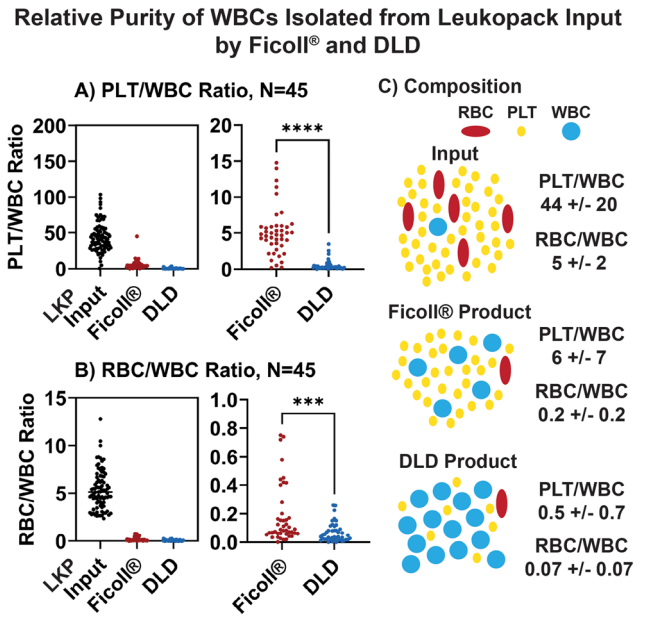

Fig. 6 Purity of the cells collected *via* microfluidic or Ficoll® preparation. A) The microfluidic DLD system yielded ~100× reduction in PLTs per WBC, *vs.* only ~10× reduction for Ficoll® ($p < 0.0001$, two-tailed *t*-test). B) The microfluidic system yielded >10× reduction in RBCs per WBC *vs.* only ~4× for Ficoll® ($p = 0.0004$, two-tailed *t*-test). C) Composition of the average leukopack input sample, Ficoll® product, and DLD product. Numerical values indicate average ± standard deviation. The microfluidic system recovered more WBCs while depleting more RBCs and PLTs, resulting in fewer contaminating cells per WBC collected and an overall purer product.

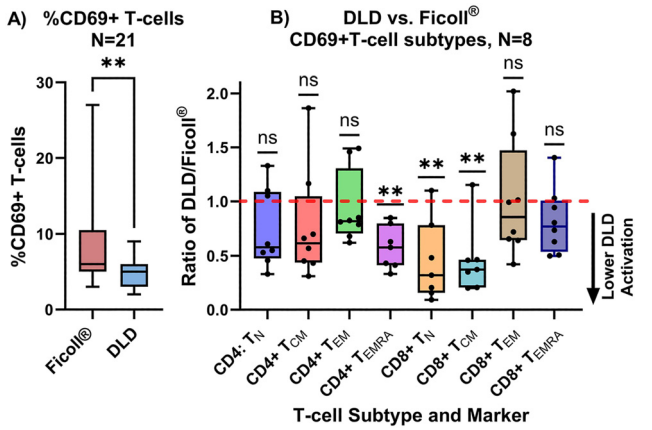

Fig. 7 A) CD69+ activation of Ficoll® *vs.* microfluidic DLD-purified cells. Ficoll® purified cells were ~2× more activated, indicated by % of CD3+ cells that are also CD69+. Box and whisker plots defined by interquartile ranges and min to max points. $p = 0.0018$, two-tailed *t*-test. B) CD69+ activation within the T cell subtypes, indicated as a ratio of DLD/Ficoll®. Ratios <1 indicate higher activation in the Ficoll®-purified cells. Box and whisker plots defined by inter-quartile ranges and min to max points. Ratios for each T cell type were compared against the theoretical value of 1 using a one-sample, two-tailed *t*-test (significance alpha = 0.05). (**) = $p < 0.01$, (ns) = not significant.

significance of 0.05, the individual ratios were compared to a theoretical value of 1. The CD4+ T_{EMRA}, CD8+ T_N and CD8+ T_{CM} samples showed a ratio significantly different than 1, indicating that the microfluidic DLD cells had lower activation within those subsets.

Washing efficiency (cytokines). To understand a potential underlying cause of the phenotype differences at day 0, cytokines from the microfluidic and Ficoll®-prepared product fractions were collected ($N = 2$ samples analyzed in duplicate, collected within 2 h of purification). A full panel analysis indicated numerous cytokines present in the Ficoll® preparation at levels exceeding 50 pg mL^{-1}, generally considered to be substantial (Fig. 8). In addition, several platelet-derived cytokines, including inhibitors of T cell proliferation like PDGF[42,43] (AA, BB and AB/BB), plus markers and mediators of cells that drive cells into senescence (PAI-1 (ref. 44)) were found at levels 5–10× higher in Ficoll® *vs.* DLD products. There were also lower levels of cytokines that reflect processing damage such as GRO-α, FGF-2 and NCAM. Some cytokines and chemokines in Ficoll® were found at levels equivalent to or higher than the starting material, possibly indicating active generation of cytokines as opposed to incomplete washing.

The input material also contained alarming levels of some cytokines and chemokines, emphasizing why an efficient, fast wash is a critical first step. The highly potent proinflammatory chemokine RANTES, produced by activated T cells and platelets, was found in the source apheresis material at a level almost 2000-fold higher than the accepted biologically active level. Following processing, Ficoll® with the manufacturer recommended two wash steps eliminated ~75% as compared to the microfluidic DLD processing, which eliminated ~95% of RANTES. While this analysis is only from a small number of samples, it highlights how the different cellular purification efficiencies combined with the degree of soluble factor elimination of potent biological response modifiers are potentially impacting activation, differentiation and response of T cells as well as other cells present.

Expansion. A randomly-selected subset of the paired samples ($N = 20$) was stimulated and expanded to observe expansion kinetics. The same number of T cells were stimulated and plated for each head-to-head comparison of microfluidic DLD and Ficoll®, and fold expansion was determined at days 3, 6, and 12. On average, by day 12 the microfluidic cells had expanded 14.7 fold *vs.* only 11.9 fold for Ficoll®, indicating almost 25% more cells in culture from the DLD-purified starting material despite plating at the same density (Fig. 9A). Using a two-tailed, paired *t*-test, the fold expansion at day 12 was found to be significantly different within the microfluidic DLD and Ficoll® populations ($p < 0.05$). To demonstrate the impact of higher recovery from the microfluidic process, the starting value at day 0 was multiplied by the %CD3+ recovery ratio (DLD/Ficoll®) for each sample (Fig. 9B). Note that the average Ficoll® %CD3+ recovery of 48 ± 16% here is lower than the $N = 86$ mean of 51.3 ± 16% but the difference between the populations is not significant. On day 0, the DLD cells began with 2.1-fold more CD3+ than Ficoll®, and by day 12 that difference grew to 2.6-fold more cells *vs.* Ficoll®. The slightly

 This journal is © The Royal Society of Chemistry 2026

Open Access Article. Published on 02 April 2026. Downloaded on 6/16/2026 12:17:03 AM.
This article is licensed under a Creative Commons Attribution-NonCommercial 3.0 Unported Licence.

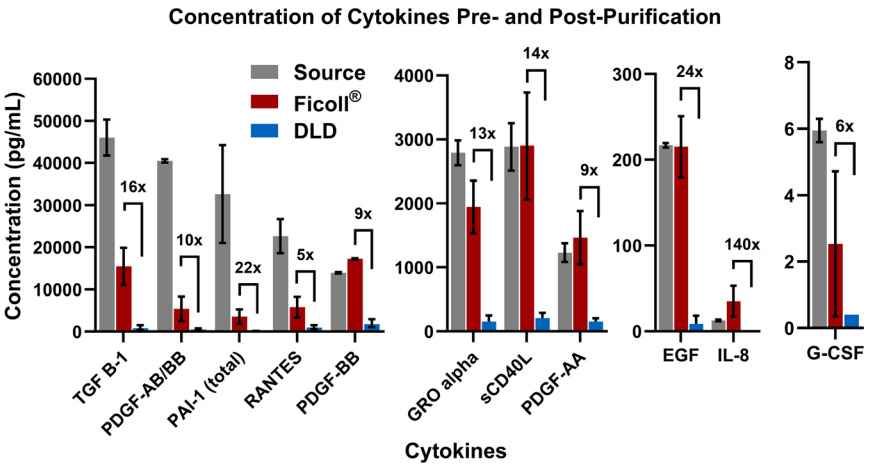

Fig. 8 Concentration of cytokines present in the environment both pre- and post-separation. $N = 2$, samples analyzed in duplicate. Shown are the instances where the ratio of Ficoll®/DLD is >5×. For PAI-1, IL-8 and G-CSF, some measurements from the DLD sample were below the assay's limit of detection. Error bars indicate standard deviation.

higher expansion kinetics, compounded by the higher initial recovery and purity of the microfluidic DLD method, resulted in the microfluidic method almost reaching the same number of cells at day 6–9 as Ficoll® reached on day 12.

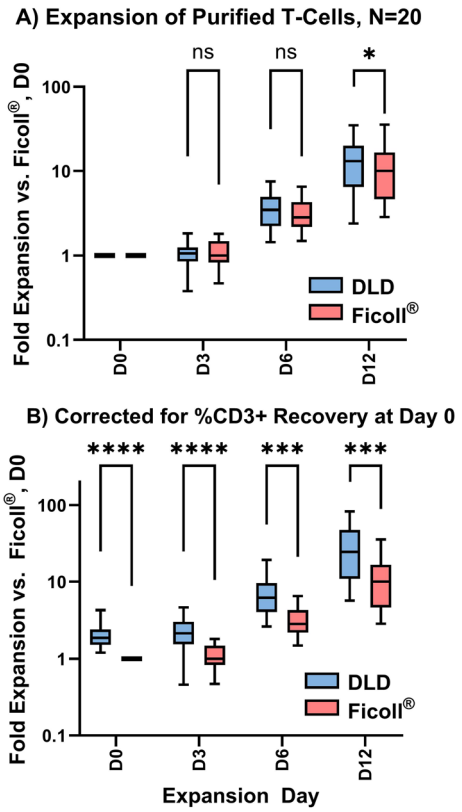

Fig. 9 A) Expansion of CD3+ cells isolated from Ficoll® and microfluidic DLD methods. At day 12, cultures from DLD-purified cells had ~25% more T cells than Ficoll®. B) Fold expansion correcting for higher %CD3+ recovery of microfluidic DLD at D0. Box and whisker plots indicate inter-quartile range and min to max points. All comparisons are paired *t*-tests for that expansion day, two-tailed, significance = 0.05. (*) = $p < 0.05$, (**) = $p < 0.01$, (***) = $p < 0.001$, (****) = $p < 0.0001$, (ns) = not significant.

Discussion

With several FDA-approved therapies already on the market, CAR-T cell therapy has emerged as a highly effective means of treating blood malignancies. For the first commercial products, a 12–25 day (or longer) manufacturing process was routine, of which 7–15 days was used for the actual manufacturing process and the rest being QC and logistics. Even today, with shorter conceptual processes, multiple steps and processes are used on day 0 to recover and purify T cells for subsequent selection and activation, which can lead to variable cell loss before the point of T cell selection.[45,46]

Here, we described a high throughput microfluidic DLD cell separation system as a method to eliminate some of the inconsistencies and impurities while minimizing losses during the earliest stages of CAR-T cell manufacturing. Inherent to DLD, size-based processing is an exceptionally efficient washing process. The single-pass separation–wash process eliminated the cell losses and forced cell–cell interactions from repeated centrifugation, and minimized non-desirable activations coming from a variety of soluble factors.

The device presented here achieved the highest WBC processivity of any microfluidic device to date. Non-equilibrium inertial arrays come close to our throughputs, showing high volumetric throughput (400 mL in less than 3 h, net ~0.2–0.5 million WBCs per s),[25] but similar devices for isolating CTCs from leukopacks have not yet demonstrated equivalent per cell metrics, with volumetric processivity (~75 mL h^{-1}) capacity (65 mL and 5 billion WBCs)[26,47] and net WBC processivity of ~1.5 million WBCs per s. Here, we demonstrated processing leukopacks up to 245 mL with up to 24 billion WBCs and at rates of up to 19 million WBCs per s. This is 5× more WBCs and a >10× improvement in the sorting

Open Access Article. Published on 02 April 2026. Downloaded on 6/16/2026 12:17:03 AM.
This article is licensed under a Creative Commons Attribution-NonCommercial 3.0 Unported Licence.

rate, achieving the end goal of full-scale processing for cell therapy applications in under an hour.

Numerous factors contributed to the consistent processing performance. Proper handling and treatment of the sample was critical: keeping the sample on a rocker at 4 °C overnight minimized platelet activity and prevented cell clumps from forming. Pre-treatment with benzonase ensured that DNA and RNA from any dead cells were degraded, minimizing the blockages and biofouling. The running buffer contained protein (BSA/HSA) which blocked the COP surface during the priming steps, helping to prevent biofouling. The upstream 20 μm filter on the cassette also played a role, removing large cell clumps before they entered the microfluidic device, protecting the micropost arrays. Most importantly, the DLD contained key features designed specifically for biologically complex, high cellularity concentrations. The array was constructed with larger gaps to increase processivity and minimize biofouling. Elongated hexagon microposts both enabled an asymmetric array geometry and maintained larger gaps for easier manufacturing. The extra array length (2× redundancy) maintained high recoveries even with very high input concentrations. Finally, the separator walls compartmentalized any biofouling, preventing product contamination.

In comparison with standard centrifugation methods, microfluidic DLD cell separation is faster and superior in terms of platelet and red blood cell reduction while requiring less manual manipulation. Efficient platelet removal is the key for CAR-T cell manufacturing where processes may induce changes in T cells and compromise their proper development.[10] The %PLT removal and CD69+ activation data shown here supports that trend with ~2× lower CD69+ activation in the DLD isolated T cells. A smaller set of samples analyzed for T cell subtypes also demonstrated a lower activation state in the DLD-prepared cells, with significantly less activation *vs.* Ficoll® demonstrated for CD4+ T_{EMRA}, CD8+ T_N and CD8+ T_{CM} cells.

Furthermore, the efficient microfluidic DLD wash process, in a small-scale study, resulted in lower levels of cytokines that negatively impact CAR-T therapies in the product. These cytokines have a range of known effects from inducing T-reg differentiation to suppressing T cell expansion and proper generation of CAR-T (Table S1 and SI data file). The reason for the lower levels of cytokines in the DLD-processed samples may be attributed to different sources. Some cytokines such as RANTES were observed in very high concentrations in the input material. RANTES is produced primarily by activated leukocytes (including T cells) during an immune response. The high level in the input material indicates that the apheresis process is causing stress. DLD processing resulted in a more complete washing of the sample, removing ~95% *vs.* only 75% for Ficoll®. However, with other cytokines, Ficoll® washing was able to achieve higher wash efficiency (Table S1). Thus, the incomplete removal of RANTES here indicates that it is still actively generated in the Ficoll® sample, supporting the hypothesis that DLD-processing is a less stressful process. Alternatively, some cytokines such as PDGF-AA and BB were at higher levels in the Ficoll® products than in the input material. These cytokines are primarily platelet-derived, which indicates that the greater removal of platelets in the DLD process is playing a role, and that the platelets in the Ficoll® sample are actively releasing cytokines. Finally, considering the panel as a whole, Ficoll® was unable to achieve the wash efficiency obtained by the DLD process, with >2× or higher levels still present. This could be attributed to active, low-level generation of cytokines in the Ficoll® sample or it could indicate a greater removal of soluble, diffusible species through microfluidic processing. Further work is required to conclusively prove any of the above hypotheses and determine the exact cause of the lower cytokines in the DLD product. Regardless, the DLD-processed cells resulted in lower levels of numerous harmful cytokines, which is particularly relevant for minimizing inflammatory responses and more severe cytokine release syndrome for shortened CAR-T processes with minimal (or no) expansion times.

While manual Ficoll® density gradient centrifugation is common in academic labs, other full-scale instrumentation is

Table 1 Performance comparison of full-scale, automated systems for WBC purification and PLT and RBC removal

Device name	Sepax™ C-Pro (Cytiva)[48–50]	CTS™ Rotea™ (Thermo Fisher)[51]	Lovo® (Fresenius Kabi)[52,53]	Curate
Technology	Centrifugation (rotating syringe)	Counterflow centrifugation (CFC)	Spinning membrane filtration	Microfluidic DLD separation
WBC recovery	>80%	>90%	97.2% (N = 5)	87 ± 6%
Platelet depletion	>80% (with 2 wash cycles)	High (exact value not stated in specifications)	98.4% (N = 5)	99 ± 1%
RBC depletion	>99% possible but with only >52% WBC recovery[49]	Partial; complete removal requires lysis buffer	~0% (limited by 4 μm pore size), requires lysis buffer	91 ± 7%
Processing time	30–120 min	25–60 min	<7–9 min (per 200 mL)	~60 min
Challenges	Tradeoff between RBC removal and WBC recovery Pellet cells (high centrifugation forces)	-Requires significant process optimization by the user -Requires lysis buffer for complete RBC removal	RBC removal requires lysis buffer	

 This journal is © The Royal Society of Chemistry 2026

Open Access Article. Published on 02 April 2026. Downloaded on 6/16/2026 12:17:03 AM. This article is licensed under a Creative Commons Attribution-NonCommercial 3.0 Unported Licence.

typically used for industrial-scale cell therapy manufacturing workflows. Systems such as Sepax™ C-Pro, (Cytiva), Gibco™ CTS™ Rotea™ (Thermo Fisher Scientific), and Lovo® (Fresenius Kabi) provide GMP-compliant, commercially available solutions. Table 1 compares the performance of those systems using the manufacturer's specifications and application notes to the performance of microfluidic DLD processing established here. Microfluidic processing matches or exceeds the performance of these systems when looking at the common comparison metrics, without exposing cells to high centrifugal forces or lysis chemicals. This performance is achieved using the same protocol for all samples processed, and without requiring any process optimization by the user.

Small scale experiments have confirmed this performance relative to full-scale systems. In a direct comparison to Rotea™ (using an RBC lysis protocol), microfluidic processing showed overall higher WBC recovery and similar purity.[15] Interestingly, after freezing and thawing, the cells prepared by the Curate system had higher yields of PBMCs and CD3 Pan-T cells after 24 and 48 h of culture. The study also confirmed the deleterious impact of ammonium chloride treatment for lysis, with the T cells processed by Rotea™ showing decreased metabolic fitness.

A second study compared microfluidic processing to Sepax™, across 6 apheresis samples.[54] Microfluidic processing on average achieved 78.7 ± 2.7% recovery of total nucleated cells, while Sepax only recovered on average 30%, a full 48% lower. When comparing T-cell recovery, the difference was even more significant, with microfluidic processing recovering 77% more CD3+ T cells. Furthermore, the difference in platelet removal between the two techniques was similar to that observed with our manual Ficoll® comparison, with microfluidic processing removing 99.7 ± 0.1% and Sepax™ removing 90.9 ± 0.6%. Similar T cell differentiation post-isolation was observed on both platforms. This study demonstrates that while current commercial systems may report higher performance in the manufacturer's specifications, the actual performance achieved by 3rd party users may be significantly different. Microfluidic processing, on the other hand, achieved the same performance, within error, as demonstrated in our large scale study.

Conclusions

Our study is the first to demonstrate full-scale microfluidic processing of apheresis samples for CAR-T cell therapy. Besides the technological advances of a microfluidic system that can operate at clinical scale and throughput, processing ~250 mL of apheresis sample in under an hour, our study shows that the inherent differences in the processing methods result in key differences in the purified products. In a field where centrifugation is the most widely used method to obtain cells, microfluidic DLD cell separation is a novel, elegant and highly efficient approach to rapidly obtain a demonstrably better starting material for downstream processing.

Author contributions

AMS: conceptualization – design of the Curate system and microfluidic arrays, investigation, supervision, formal analysis, writing – original draft, review and editing, visualization, and funding acquisition. YB: conceptualization – design of the Curate system and microfluidic arrays, investigation, data curation, supervision, and resources. LP: investigation and formal analysis. DI: conceptualization – design of the microfluidic arrays and writing – review and editing. MS: investigation. LO: investigation. KG: conceptualization – design of the Curate system and microfluidic arrays, supervision, project administration, and funding acquisition. RCG: investigation, supervision, resources, writing – original draft, review and editing, and funding acquisition. TW: conceptualization – design of the Curate system and microfluidic arrays, investigation, supervision, formal analysis, writing – original draft, review and editing, and funding acquisition.

Conflicts of interest

Alison M. Skelley, Yasna Behmardi, Luke Peterson, Mabel Shehada, Laurissa Ouaguia, Khushroo Gandhi, Roberto Campos-Gonzales, and Tony Ward were all employees of Curate Biosciences and inventors on patents owned by Curate Biosciences. Alison M. Skelley is a current employee of Zeon Specialty Materials, a subsidiary of Zeon Corporation which acquired IP from Curate Biosciences. Tony Ward is a consultant to companies in the field of cell therapy, some of which are evaluating different systems for cell purification.

Glossary

DLD	Deterministic lateral displacement
DCS	Deterministic cell separation
PBS	Phosphate buffered saline
PLA	Plasmalyte-A
LKP	Leukopack, standard apheresis unit
WBC	White blood cell
RBC	Red blood cell
PLT	Platelet
BSA	Bovine serum albumin
HSA	Human serum albumin
ACD-A	Anticoagulant citrate dextrose solution, solution A
COP	Cyclo olefin polymer

Data availability

The datasets generated during and/or analyzed during the current study are available at https://doi.org/10.5061/dryad.m37pvmdhj.

Supplementary information (SI) is available. See DOI: https://doi.org/10.1039/d6lc00072j.

Open Access Article. Published on 02 April 2026. Downloaded on 6/16/2026 12:17:03 AM. This article is licensed under a Creative Commons Attribution-NonCommercial 3.0 Unported Licence.

Acknowledgements

This study was funded in part by NIH STTR Grant R42-CA228616 Microfluidic CAR-T Cell Processing Device. https://reporter.nih.gov/search/xrXH0tDULkiksJ1gOETscg/project-details/9554166. We are grateful to Chris Boyce for his assistance in analyzing flow cytometry data and compiling summaries. We also wish to acknowledge the thoughtful input from Dr. Curt Civin at the University of Maryland Baltimore and Dr. James Sturm of Princeton University, both of whom were also funded by the STTR.

References

1 G. Choi, G. Shin and S. Bae, Price and Prejudice? The Value of Chimeric Antigen Receptor (CAR) T-Cell Therapy, *Int. J. Environ. Res. Public Health*, 2022, **19**, 12366.
2 A. Melocchi, *et al.*, Automated manufacturing of cell therapies, *J. Controlled Release*, 2025, **381**, 113561.
3 M. Di, *et al.*, Total Costs of Care during Chimeric Antigen Receptor T-Cell Therapy in Patients with Relapsed/Refractory B Cell Non-Hodgkin Lymphoma: A Large Private Insurance Claim-Based Analysis, *Blood*, 2022, **140**, 10818–10819.
4 Patient Access Tracker, Oribiotech Ltd, https://oribiotech.com/insight/patient-access-tracker.
5 Time to CAR T cell Therapy May Impact Outcomes for Patients With RelapsedRefractory Large B cell Lymphoma in New CIBMTR Analysis, https://www.gilead.com/news/news-details/2022/time-to-car-t-cell-therapy-may-impact-outcomes-for-patients-with-relapsedrefractory-large-b-cell-lymphoma-in-new-cibmtr-analysis.
6 T. Kourelis, *et al.*, Ethical Challenges with Multiple Myeloma BCMA Chimeric Antigen Receptor T Cell Slot Allocation: A Multi-Institution Experience, *Transplant. Cell. Ther.*, 2023, **29**, 255–258.
7 M. Ayala Ceja, M. Khericha, C. M. Harris, C. Puig-Saus and Y. Y. Chen, CAR-T cell manufacturing: Major process parameters and next-generation strategies, *J. Exp. Med.*, 2024, **221**, e20230903.
8 St. Martin, Y., Franz, J. K., Agha, M. E. & Lazarus, H. M., Failure of CAR-T cell therapy in relapsed and refractory large cell lymphoma and multiple myeloma: An urgent unmet need, *Blood Rev.*, 2023, **60**, 101095.
9 S. T. Bhaskar, B. R. Dholaria, S. M. Sengsayadeth, B. N. Savani and O. O. Oluwole, Role of bridging therapy during chimeric antigen receptor T cell therapy, *eJHaem*, 2022, **3**, 39–45.
10 C. Polasky, F. Wendt, R. Pries and B. Wollenberg, Platelet Induced Functional Alteration of CD4+ and CD8+ T Cells in HNSCC, *Int. J. Mol. Sci.*, 2020, **21**, 7507.
11 S. G. Gray and T. J. Ekström, Effects of Cell Density and Trichostatin A on the Expression ofHDAC1andp57Kip2in Hep 3B Cells, *Biochem. Biophys. Res. Commun.*, 1998, **245**, 423–427.
12 T. Akimova, U. H. Beier, Y. Liu, L. Wang and W. W. Hancock, Histone/protein deacetylases and T-cell immune responses, *Blood*, 2012, **119**, 2443–2451.
13 J. Domagala, *et al.*, Ammonia Suppresses the Antitumor Activity of Natural Killer Cells and T Cells by Decreasing Mature Perforin, *Cancer Res.*, 2025, **85**, 2448–2467.
14 Z. Li, *et al.*, The Impact of Ammonium Chloride-Based Erythrocyte Lysis Process on Banked Adipose-Derived Stem Cells, *Biopreserv. Biobanking*, 2022, **20**, 229–237.
15 R. J. Tressler, T. Cabreros, M. Tran, A. Thind and A. Ward, Adverse Impact of NH4Cl-Based Erythroreduction On T Cells, *Cytotherapy*, 2025, **27**, S205–S206.
16 O. C. Finney, *et al.*, CD19 CAR T cell product and disease attributes predict leukemia remission durability, *J. Clin. Invest.*, 2019, **129**, 2123–2132.
17 S. Ghassemi, *et al.*, Reducing Ex Vivo Culture Improves the Antileukemic Activity of Chimeric Antigen Receptor (CAR) T Cells, *Cancer Immunol. Res.*, 2018, **6**, 1100–1109.
18 J. A. Fraietta, *et al.*, cDeterminants of response and resistance to CD19 chimeric antigen receptor (CAR) T cell therapy of chronic lymphocytic leukemia, *Nat. Med.*, 2018, **24**, 563–571.
19 C. U. Louis, *et al.*, Antitumor activity and long-term fate of chimeric antigen receptor–positive T cells in patients with neuroblastoma, *Blood*, 2011, **118**, 6050–6056.
20 Z. Bai, *et al.*, Single-cell antigen-specific landscape of CAR T infusion product identifies determinants of CD19-positive relapse in patients with ALL, *Sci. Adv.*, 2022, **8**, eabj2820.
21 Y. Sun, *et al.*, Depletion of Tregs from CD4+ CAR-T cells enhances the tumoricidal effect of CD8+ CAR-T cells in anti-CD19 CAR-T therapy, *FEBS J.*, 2025, **292**, 1904–1919.
22 J. D'Silva, R. H. Austin and J. C. Sturm, Inhibition of clot formation in deterministic lateral displacement arrays for processing large volumes of blood for rare cell capture, *Lab Chip*, 2015, **15**, 2240–2247.
23 M. E. Warkiani, *et al.*, Ultra-fast, label-free isolation of circulating tumor cells from blood using spiral microfluidics, *Nat. Protoc.*, 2016, **11**, 134–148.
24 A. J. Mach and D. Di Carlo, Continuous scalable blood filtration device using inertial microfluidics, *Biotechnol. Bioeng.*, 2010, **107**, 302–311.
25 B. R. Mutlu, *et al.*, Non-equilibrium Inertial Separation Array for High-throughput, Large-volume Blood Fractionation, *Sci. Rep.*, 2017, **7**, 9915.
26 A. Mishra, *et al.*, Tumor cell-based liquid biopsy using high-throughput microfluidic enrichment of entire leukapheresis product, *Nat. Commun.*, 2025, **16**, 32.
27 S. Sheybanikashani, J. Zhou and I. Papautsky, Blood microfluidics: progress and challenges, *Lab Chip*, 2026, **26**, 1123–1147.
28 J. L. Duncan, J. P. Arroyo and R. V. Davalos, Microfluidics for cell therapy and manufacturing in oncology and regenerative medicine, *Lab Chip*, 2026, **26**, 1566–1587.
29 Z. Wang and S. O. Kelley, Microfluidic technologies for enhancing the potency, predictability and affordability of adoptive cell therapies, *Nat. Biomed. Eng.*, 2025, **9**, 803–821.
30 R. Campos-González, *et al.*, Deterministic Lateral Displacement: The Next-Generation CAR T-Cell Processing?, *SLAS Technol.*, 2018, **23**, 338–351.

 This journal is © The Royal Society of Chemistry 2026

Open Access Article. Published on 02 April 2026. Downloaded on 6/16/2026 12:17:03 AM. This article is licensed under a Creative Commons Attribution-NonCommercial 3.0 Unported Licence.

31 T. Ward, A. Skelley, K. Gandhi and R. Campos-González, Efficient production of T-central memory cells from apheresis product using microfluidic chips, *Cytotherapy*, 2018, **20**, S98.
32 Ficoll-Paque PLUS, https://cdn.cytivalifesciences.com/api/public/content/digi-12637-original.
33 T. F. Scientific CTS Dynabeads CD3/CD28, https://documents.thermofisher.com/TFS-Assets/LSG/manuals/11131D_32D_61D.pdf.
34 D. W. Inglis, J. A. Davis, R. H. Austin and J. C. Sturm, Critical particle size for fractionation by deterministic lateral displacement, *Lab Chip*, 2006, **6**, 655–658.
35 K. K. Zeming, T. Salafi, C.-H. Chen and Y. Zhang, Asymmetrical Deterministic Lateral Displacement Gaps for Dual Functions of Enhanced Separation and Throughput of Red Blood Cells, *Sci. Rep.*, 2016, **6**, 22934.
36 M. Al-Fandi, M. Al-Rousan, M. A. K. Jaradat and L. Al-Ebbini, New design for the separation of microorganisms using microfluidic deterministic lateral displacement, *Robot. Cim-Int. Manuf.*, 2011, **27**, 237–244.
37 Y. Chen, J. D'Silva, R. H. Austin and J. C. Sturm, Microfluidic chemical processing with on-chip washing by deterministic lateral displacement arrays with separator walls, *Biomicrofluidics*, 2015, **9**(5), 054105.
38 D. Inglis, R. Vernekar, T. Krüger and S. Feng, The fluidic resistance of an array of obstacles and a method for improving boundaries in deterministic lateral displacement arrays, *Microfluid. Nanofluid.*, 2020, **24**, 18.
39 S. L. Feng, A. M. Skelley, A. G. Anwer, G. Liu and D. W. Inglis, Maximizing particle concentration in deterministic lateral displacement arrays, *Biomicrofluidics*, 2017, **11**, 024121.
40 Y. D. Mahnke, T. M. Brodie, F. Sallusto, M. Roederer and E. Lugli, The who's who of T-cell differentiation: Human memory T-cell subsets, *Eur. J. Immunol.*, 2013, **43**, 2797–2809.
41 M. Schmueck-Henneresse, *et al.*, Comprehensive approach for identifying the T-cell subset origin of CD3 and CD28 antibody-activated chimeric antigen receptor-modified T-cells, *J. Immunol.*, 2017, **199**, 348–362.
42 R. A. Daynes, T. Dowell and B. A. Araneo, Platelet-derived growth factor is a potent biologic response modifier of T cells, *J. Exp. Med.*, 1991, **174**, 1323–1333.
43 C.-F. Chen, *et al.*, Regulation of T cell proliferation by JMJD6 and PDGF-BB during chronic hepatitis B infection, *Sci. Rep.*, 2014, **4**, 6359.
44 D. E. Vaughan, R. Rai, S. S. Khan, M. Eren and A. K. Ghosh, Plasminogen Activator Inhibitor-1 Is a Marker and a Mediator of Senescence, *Arterioscler., Thromb., Vasc. Biol.*, 2017, **37**, 1446–1452.
45 O. L. Reddy, D. F. Stroncek and S. R. Panch, Improving CAR T cell therapy by optimizing critical quality attributes, *Semin. Hematol.*, 2020, **57**, 33–38.
46 H. W. Song, *et al.*, CAR-T cell expansion platforms yield distinct T cell differentiation states, *Cytotherapy*, 2024, **26**, 757–768.
47 A. Mishra, *et al.*, Ultrahigh-throughput magnetic sorting of large blood volumes for epitope-agnostic isolation of circulating tumor cells, *Proc. Natl. Acad. Sci. U. S. A.*, 2020, **117**, 16839–16847.
48 PlateletFree C-Pro application software, https://cdn.cytivalifesciences.com/api/public/content/digi-26896-pdf.
49 NeatCell C-Pro application software, https://cdn.cytivalifesciences.com/api/public/content/digi-31044-pdf.
50 V. A. Remley, *et al.*, Optimizing a fully automated and closed system process for red blood cell reduction of human bone marrow products, *Cytotherapy*, 2023, **25**, 442–450.
51 CTS Gibco Rotea Counterflow Centrifugation System Specifications, https://www.thermofisher.com/us/en/home/clinical/cell-gene-therapy/cell-therapy/cell-therapy-manufacturing-solutions/rotea-counterflow-centrifugation-system/sample-data.html.
52 Lovo® Cell Processing System Simple, Flexible, and Scalable Automated Cell Processing, https://www.fresenius-kabi.com/content/dam/fresenius-kabi/us/documents/products/medtech/brochures/Lovo%20General%20Brochure.pdf.coredownload.inline.pdf.
53 Lovo Automated Cell Processing System The easy-to-use, flexible, filtered way to wash and volume-reduce white blood cells, https://www.fresenius-kabi.com/content/dam/fresenius-kabi/ca/products/product-documents/transfusion-technology/cell-therapy-technologies/3132D_lovo_brochure.pdf.
54 H. W. Song, *et al.*, MICROFLUIDIC SEPARATION TECHNOLOGY IMPROVES PURITY AND YIELD OF PBMCS FOR CELL MANUFACTURING APPLICATIONS, *Cytotherapy*, 2024, **26**, S26.